

Cite this article as: Chen Wenxuan, Zhou Guorong, Wang Xuefeng, et al. Effect of Adding RE and Ti Elements on Microstructure and Corrosion Resistance of Zn-2.5Al-3Mg Alloy[J]. Rare Metal Materials and Engineering, 2023, 52(08): 2737-2745.

ARTICLE

Effect of Adding RE and Ti Elements on Microstructure and Corrosion Resistance of Zn-2.5Al-3Mg Alloy

Chen Wenxuan¹, Zhou Guorong¹, Wang Xuefeng¹, Ma Longyue¹, Zhao Degang¹, Li Yongsheng², Wang Dong², Qin Bilian³

¹ School of Materials Science and Engineering, University of Jinan, Jinan 250022, China; ² Shandong Quality Inspection and Testing Center of Construction Engineering Co., Ltd, Jinan 250031, China; ³ Shandong Huankeyuan Environmental Engineering Co., Ltd, Jinan 250013, China

Abstract: The effect of addition of RE and Ti on the microstructure and corrosion resistance of Zn-2.5Al-3Mg alloy were investigated by XRD, SEM, TEM and XPS. Results reveal that the microstructure of the Zn-2.5Al-3Mg alloy is composed of Zn-rich phase, binary eutectic (Zn-MgZn₂/Mg₂Zn₁₁) and ternary eutectic (Zn/Al/Mg₂Zn₁₁). New phases of (Ce_{1-x}La_x)Zn₁₁ and Al₂Ti appear with the addition of RE and Ti elements. Electrochemical impedance spectroscopy indicates that the corrosion resistance of Zn-2.5Al-3Mg-0.1RE-0.2Ti alloy can be significantly improved compared to that of Zn-2.5Al-3Mg alloy. XPS analysis results show that the addition of RE element promotes the formation of Zn₅(CO₃)₂(OH)₆ and MgAl₂O₄ in the corrosion products, while the simultaneous addition of RE and Ti elements promotes the formation of corrosion products Zn₅(CO₃)₂(OH)₆, ZnAl₂O₄ and MgAl₂O₄, and inhibits the formation of loose porous ZnO. Zn₅(CO₃)₂(OH)₆, ZnAl₂O₄ and MgAl₂O₄ attach well to the surface of the sample, which provides a dense protective layer for the alloys, thus improving the corrosion resistance of Zn-2.5Al-3Mg alloy.

Key words: Zn-Al-Mg alloy; corrosion resistance; electrochemistry; XPS

With the increasing demands for the corrosion resistance of steel in industry, the traditional hot-dip galvanizing cannot meet the demand. The corrosion resistance of the alloy can be further improved by the addition of alloying element like aluminum^[1-2], such as Galfan coatings, of which the corrosion resistance is about three times higher than that of pure zinc coatings, which has been widely used in construction, automotive processing and other fields^[3-4]. At present, Zn-Al-Mg series coatings have been extensively studied, due to their corrosion resistance superior to that of traditional Zn and Zn-Al series coatings^[5-7].

In the past 20 years, many Zn-Al-Mg alloys have been studied, such as the famous ZAM (Zn-6Al-3Mg) produced by Nissin steel corporation of Japan^[8] and PosMAC (Zn-2.5Al-3Mg) produced by POSCO of South Korea^[9]. In order to expand the application and to prolong the service life of Zn-Al-Mg alloy, researchers begin to study the effect of element addition on Zn-Al-Mg alloy. Li et al^[10] found that the addition of RE can homogenize the structure of Zn-6Al-3Mg alloy and

inhibit intergranular corrosion. Guo et al^[11] studied the influence of electrochemical properties on surface micromorphology of Zn-Al-Mg-RE alloy coatings. It is found that the addition of RE can improve the corrosion resistance of the alloy. Han et al^[12] studied the effect of RE co-doping on corrosion behavior of Zn-Al-Mg hot-dip galvanizing coatings used for transmission towers. It was found that the addition of RE can refine the microstructure of Zn-Al-Mg alloy, and then significantly improve the corrosion resistance of the alloy.

In addition, Ti is a metal with relatively strong passive stability and can form a protective oxide film^[13-14]. Dong et al^[15] found that adding Ti element to Zn-55Al alloy can significantly improve the corrosion resistance of the alloy. Cui et al^[16] found that the self-corrosion current density of Zn-5Al-0.15Ti alloy coating is smaller than that of Zn-5Al alloy coating, demonstrating that the addition of Ti can slow down the corrosion of the alloy. However, there is little report on the effect of adding RE and Ti simultaneously on the microstructure and corrosion resistance of Zn-Al-Mg alloy.

Received date: December 03, 2022

Foundation item: Natural Science Foundation of Shandong Province (ZR2021ME191)

Corresponding author: Zhou Guorong, Ph. D., School of Materials Science and Engineering, University of Jinan, Jinan 250022, P. R. China, Tel: 0086-531-82765473, E-mail: mse_zhougr@ujn.edu.cn

Copyright © 2023, Northwest Institute for Nonferrous Metal Research. Published by Science Press. All rights reserved.

Therefore, the aim of this work is to investigate the effect of RE and Ti on the microstructure and corrosion behavior of Zn-Al-Mg alloy.

1 Experiment

Zn-2.5Al-3Mg, Zn-2.5Al-3Mg-0.1RE (RE refers to La and Ce) and Zn-2.5Al-3Mg-0.1RE- x Ti ($x=0.1, 0.2, 0.3, 0.4$) alloys were prepared by casting method. The metals of Zn (99.99wt%), Al (99.5wt%), Mg (99.99wt%), Mg-20RE and Al-15Ti were melted in electrical resistance furnace at 750 °C for 2 h for dissolving and homogenizing. Afterwards, the melt was cooled to 550 °C and kept for a certain time. Finally, the melt was cast into the mold under atmospheric conditions to obtain the alloy ingot required for the experiment.

The microstructure of prepared specimens was observed by scanning electron microscope (SEM; FEG-250) equipped with back scattered electron (BSE). The energy dispersive spectroscopy (EDS) attached to SEM was used to analyze the elemental composition of the alloys. The characterization was performed by transmission electron microscope (TEM; JEM-2100) equipped with EDS. Additionally, the phase was identified by X-ray diffraction (XRD; D8 advance). A step-scan mode was used at the 2θ range from 10° to 90°.

The electrochemical measurements were conducted on IM6d Zahner-Elektrok workstation. Three-electrode system composed of working electrode (Zn-based alloys with 1cm² in test surface), counter electrode (Pt electrode) and reference electrode (saturated calomel electrode, SCE) was used to evaluate the corrosion behavior of the alloys. Electrochemical impedance spectroscopy (EIS) test was conducted under the sinusoidal potential perturbation of ± 10 mV in the frequency range of 10⁻¹ Hz to 10¹ mHz. The samples were subjected to dynamic polarization after stabilizing the open circuit potential (OCP) for 30 min in all the experiments. The scanning rate of dynamic polarization was 10 mV/s. All electrochemical measurements were conducted in the 3.5wt% NaCl solution at room temperature. The surface corrosion products of the alloys were analyzed by X-ray photoelectron spectroscopy (XPS; ESCALAB Xi+). The fitting procedure was carried out by Avantage software considering linear background, and C 1s peak of adventitious carbon at a binding energy of 284.8 eV was used to normalize the absolute energy.

2 Results and Discussion

2.1 Microstructure characteristics

The XRD patterns of Zn-2.5Al-3Mg, Zn-2.5Al-3Mg-0.1RE and Zn-2.5Al-3Mg-0.1RE-0.2Ti alloys are presented in Fig. 1. It should be noted that Zn, MgZn₂, Mg₂Zn₁₁ phases are identified in all alloys^[17-18]. The addition of Ti in Zn-2.5Al-3Mg-0.1RE leads to new phase (Al₂Ti). The diffraction peaks of Al and RE are not detected, which may be due to the lower content or the formation of fewer phases. There is a strong preferred orientation because the samples are as-cast. Zn has the preferential orientations of Zn (0002), Zn (10 $\bar{1}$ 0) and Zn (10 $\bar{1}$ 1) at 2θ value of 36°, 39° and 43°, respectively.

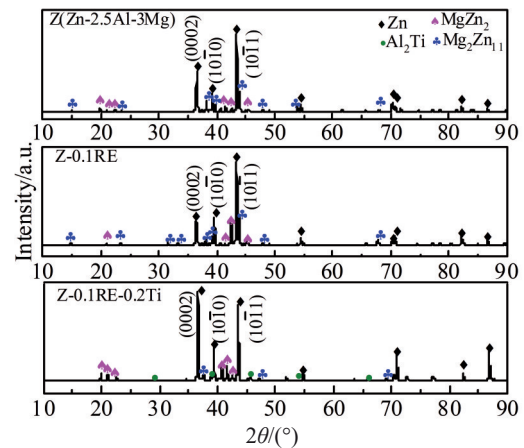


Fig.1 XRD patterns of Zn-2.5Al-3Mg, Zn-2.5Al-3Mg-0.1RE and Zn-2.5Al-3Mg-0.1RE-0.2Ti alloys

The microstructure of Zn-2.5Al-3Mg alloy is shown in Fig. 2. The EDS data of the points marked in Fig. 2 are presented in Table 1. It can be found that the microstructure of the Zn-2.5Al-3Mg alloy is composed of Zn-rich phase, binary eutectic and ternary eutectic. EDS analyses in Table 1 reveal that the compositions of the black area (point 1), bright white area (point 2), and light grey area (point 3) in the binary eutectic (Fig. 2a) are MgZn₂, Zn-rich, Mg₂Zn₁₁ phases respectively. Based on the phase diagram of Zn-Al-Mg alloy, MgZn₂ phase firstly forms as the primary phase and then transforms to Mg₂Zn₁₁ in the peritectic reaction: MgZn₂+L→Mg₂Zn₁₁^[19-20]. However, this transition is different from the actual crystallization rate, so the microstructure of the alloy shows that the MgZn₂ phase is surrounded by Mg₂Zn₁₁ phase (Fig. 2a). Fig. 2b shows the enlarged region of the ternary

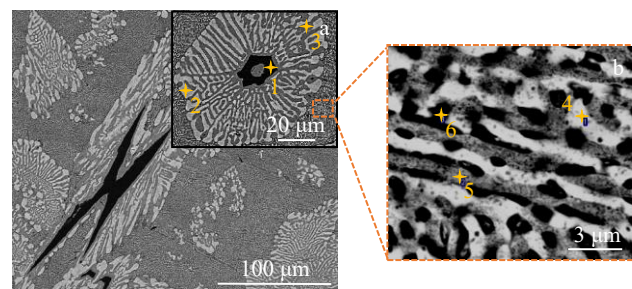


Fig.2 Microstructure (a) and EDS analysis points of Zn-2.5Al-3Mg alloy

Table 1 EDS results of different points marked in Fig.2 (at%)

Point	Zn	Al	Mg
1	63.17	1.68	35.15
2	97.66	2.34	-
3	82.47	3.30	14.24
4	88.66	7.05	4.29
5	77.71	8.55	13.74
6	69.50	26.23	4.27

eutectic. Combined with EDS analysis results, the ternary eutectic consists of Zn, Al, Mg_2Zn_{11} phases. As observed in Fig.2b, the Zn-rich phase and Mg_2Zn_{11} phase are distributed in layers, while the black granular Al-rich phase is attached between them.

Fig.3 presents the surface morphologies of Zn-2.5Al-3Mg-0.1RE-xTi ($x=0, 0.1, 0.2, 0.3, 0.4$) alloys. The phase compositions of the alloys are determined by EDS, and corresponding results are illustrated in Table 2. As indicated in Fig.3, the addition of RE and Ti elements cannot change the microstructure of the alloy. However, the phase composition is different from that of Zn-2.5Al-3Mg alloy. Zn-2.5Al-3Mg-0.1RE alloy is composed of primary Zn, binary eutectic (Zn- $MgZn_2/Mg_2Zn_{11}$), ternary eutectic (Zn/Al/ Mg_2Zn_{11}), and white massive phase. Combined with EDS results in Table 2 (point 1), it suggests that the white massive phase is $(Ce_{1-x}La_x)Zn_{11}$ ($x=0.41$)^[21]. The phase composition of the Ti-added alloy is similar to that of Zn-2.5Al-3Mg-0.1RE, and the difference is that there are primary Al phase (point 4 in Table 2) and black regular objects. The atomic ration of the black regular object is close to Al:Ti=2:1 (point 3 in Table 2), so it is considered as Al_2Ti phase. This result is consistent with XRD analysis in Fig.1.

As shown in Fig.3a–3e, when RE element is added to Zn-2.5Al-3Mg alloy alone, the average grain size of binary

eutectic structure is almost the same as that without RE element. However, after the addition of Ti, the grain size of binary eutectic structure is significantly reduced (marked by white circles in Fig. 3a – 3e), and its number is also significantly increased. Meanwhile, it can also be clearly observed that granular Al-rich phase is distributed at the grain boundary of binary eutectic grains (yellow arrows marked in Fig.3b–3e). Moreover, with the increase in Ti element ($Y=0.1–0.4$), the grain size of binary eutectic structure first decreases and then increases. When $X=0.2$, the amount of $MgZn_2$ phase reaches the maximum in all six alloys. Some studies have proved that the existence of $MgZn_2$ phase can greatly improve the corrosion resistance of the alloy^[22–23]. In other words, the corrosion resistance of Zn-2.5Al-3Mg-0.1RE-0.2Ti alloy may be the best among the six alloys, which needs to be further proved by the subsequent electrochemical performance analysis.

The EDS mapping of Zn-2.5Al-3Mg, Zn-2.5Al-3Mg-0.1RE and Zn-2.5Al-3Mg-0.1RE-0.2Ti alloys are shown in Fig.4. As observed in Fig.4a, the Al-rich phase is mainly distributed in the ternary eutectic structure, and the Mg and Zn elements combine to form the $MgZn_x$ phase. In the Zn-2.5Al-3Mg-0.1RE alloy, the distribution of Al and Mg elements is similar to that of Zn-2.5Al-3Mg. The white hexagonal object is mainly composed of Zn, La and Ce elements (Fig. 4b). Ti

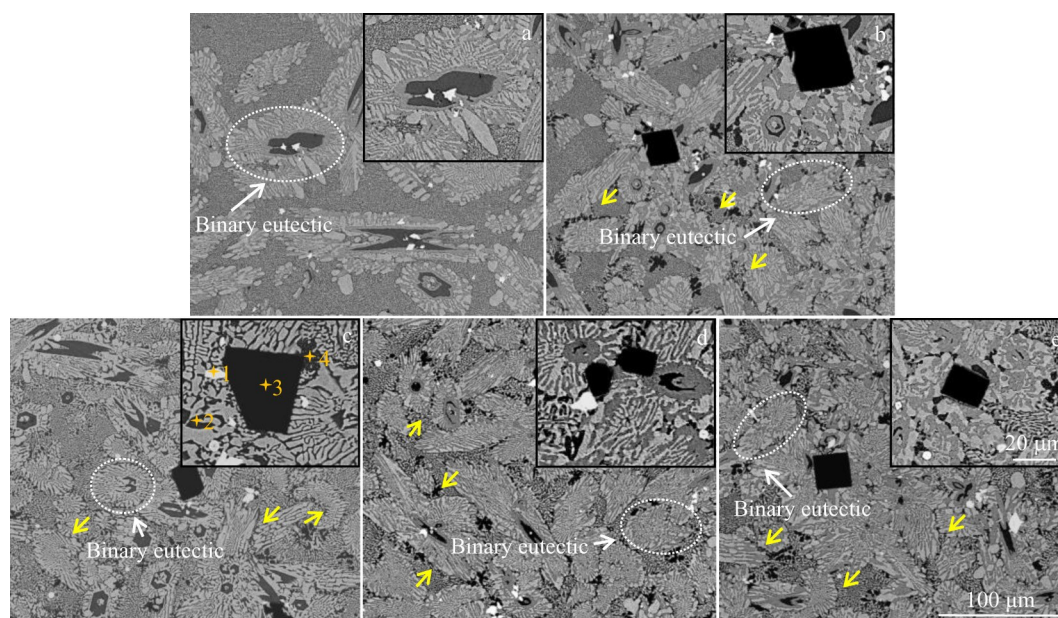


Fig.3 SEM microstructures of Zn-2.5Al-3Mg-0.1RE-xTi alloys: (a) $x=0$, (b) $x=0.1$, (c) $x=0.2$, (d) $x=0.3$, and (e) $x=0.4$

element is mainly combined with Al to form $AlTi_x$ phase in the alloys containing Ti element. In comparison, it is obviously observed that granular Al-rich phase is distributed at the grain boundary of binary eutectic grains in the alloys containing Ti element (marked with yellow arrows). In addition, the distribution of Al element is in the same ternary eutectic structure as that in Zn-2.5Al-3Mg and Zn-2.5Al-3Mg-0.1RE alloys.

Table 2 EDS results of points marked in Fig.3c (at%)

Point	Zn	Al	Mg	Ti	La	Ce
1	89.53	2.21	-	-	3.35	4.91
2	68.58	1.80	29.62	-	-	-
3	23.94	50.87	0.12	24.88	0.09	0.10
4	54.77	45.23	-	-	-	-

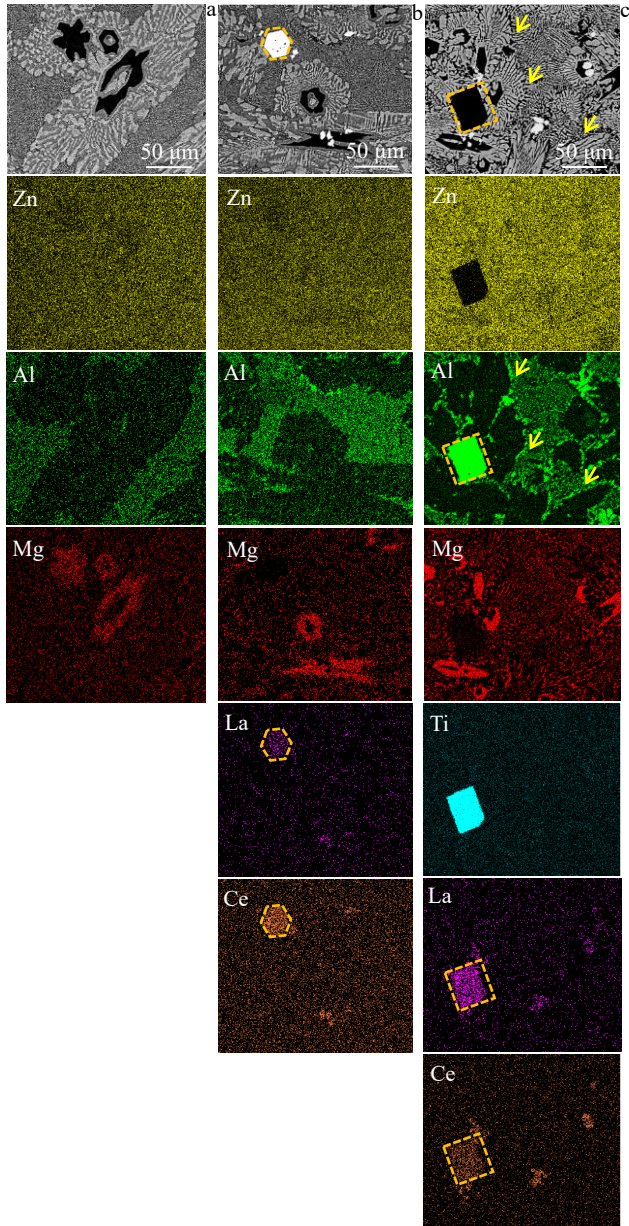


Fig.4 EDS mappings of Zn-2.5Al-3Mg (a), Zn-2.5Al-3Mg-0.1RE (b) and Zn-2.5Al-3Mg-0.1RE-0.2Ti (c) alloys

In order to further analyze the phase structure of the alloys added with RE and Ti elements, the Zn-2.5Al-3Mg-0.1RE-0.2Ti alloy was selected for TEM analysis, and the results are shown in Fig.5. The electron diffraction spots in regions 1, 2, 3 and 4 in Fig.5a correspond to Fig.5c–5f, respectively. The crystal face indexes are (0002), ($\bar{1}011$), ($\bar{1}010$) in the region 1, so the region 1 is hcp-Zn solid solution. The crystal face indexes in the region 2 are (111), (200), ($1\bar{1}\bar{1}$), which is a solid solution of fcc-Al. The crystal face indexes of solid solution are (120), (320), (200) in the region 3, and the pattern is consistent with [004] Mg_2Zn_{11} . Therefore, it is identified as the Mg_2Zn_{11} phase. The crystal face indexes of region 4 are ($10\bar{1}0$), ($10\bar{1}3$), (0003), which is a solid solution of hexagonal $MgZn_2$ phase. Veys-Renaux et al.^[21] described the substitution of Ce with La at constant Zn ratio, treated as the formula

$(Ce, La)_aZn_b$ in the Ce-La-Zn ternary system. The bright-filed image of the TEM of the $(Ce, La)_aZn_b$ phase is shown in Fig. 5b, and the corresponding EDS results are presented in Fig.5g. The atomic ratio of Ce and La elements to Zn element is close to 1:11, so the phase is identified as the $(Ce_{1-x}La_x)Zn_{11}$ phase. The results are consistent with SEM analysis (Fig.3).

2.2 Electrochemical impedance spectroscopy (EIS)

The corrosion behavior of the six alloys in 3.5wt% NaCl solution was studied by electrochemical impedance measurements, and the Nyquist and Bode plots are shown in Fig.6. The Bode phase angle diagram in Fig.6b shows the wave crest in a frequency range of $10^2 - 10^3$ Hz for tested specimens, indicating that the corrosion mechanisms of the six alloys are the same. Additionally, it is clearly found that the capacitance arc radius of the alloys with RE and Ti elements is larger than that of the Zn-2.5Al-3Mg alloy in Fig.6a. The larger the capacitance arc radius, the higher the charge transfer resistance, and the more difficult the corrosion of the alloy^[24-25]. Moreover, Bode modulus plots in Fig. 6c suggest that impedance of the alloys with RE and Ti elements is higher than that of the Zn-2.5Al-3Mg alloy. The results indicate that the addition of RE and Ti elements can significantly improve the corrosion resistance of Zn-2.5Al-3Mg alloy.

To compare the corrosion resistance of the six alloys more intuitively, a fitting equivalent circuit mode is given in Fig.6d based on the EIS data. Table 3 shows the fitting results. In Fig. 6d, R_s is the solution resistance, R_f is the resistance of surface products, and R_{ct} is the charge transfer resistance. CPE_1 and CPE_2 are constant phase angle elements, referring to the capacitance of the surface product layer and double layer, respectively. n represents the dispersion coefficient, and its dimensionless parameter range is $0-1$ ^[26-28]. The solution resistance R_s of all samples is not only are lower than $10 \Omega \cdot cm^2$, but also much lower than R_f and R_{ct} . This indicates that all samples are in a stable testing environment^[17]. It is worth noting that the corrosion product resistance R_f of the Zn-2.5Al-3Mg-0.1RE-0.2Ti alloy is higher than that of other alloys, indicating that the corrosion product layer of Zn-2.5Al-3Mg-0.1RE-0.2Ti alloy is more compact than that of other alloys. In addition, the R_{ct} of the Zn-2.5Al-3Mg-0.1RE-0.2Ti alloy is also higher than that of other alloys, indicating that it is more difficult to corrode. Therefore, the corrosion resistance of Zn-2.5Al-3Mg-0.1RE-0.2Ti alloy is the best among these alloys.

2.3 Potentiodynamic polarization

Comparison of polarization curves of Zn-2.5Al-3Mg, Zn-2.5Al-3Mg-0.1RE and Zn-2.5Al-3Mg-0.1RE- x Ti alloys in 3.5wt% NaCl solution is shown in Fig. 7. The corrosion potential E_{corr} and the corrosion current density I_{corr} can be obtained by Tafel extrapolation, and the corresponding values are shown in Table 4. The corrosion potential and the corrosion current density of Zn-2.5Al-3Mg are -1.534 V and 1.2942×10^{-4} A/cm², respectively. It is clearly observed that corrosion potential of the alloys added with RE and Ti elements is considerably larger (positive) as compared to that of Zn-2.5Al-3Mg alloy, and the corrosion current density is

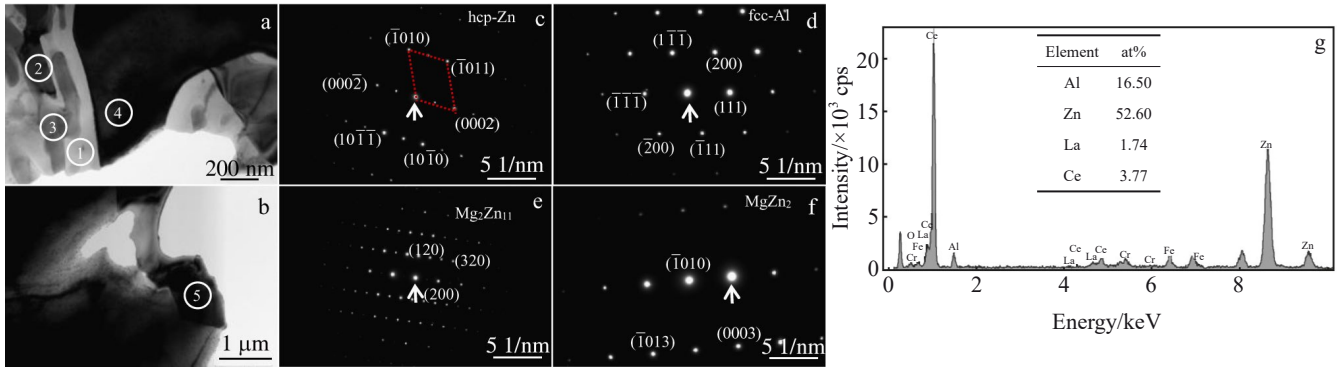


Fig.5 TEM images of Zn-2.5Al-3Mg-0.1RE-0.2Ti alloy (a, b); corresponding SAED patterns of region 1 (c), region 2 (d), region 3 (e) and region 4 (f); EDS result of region 5 (g)

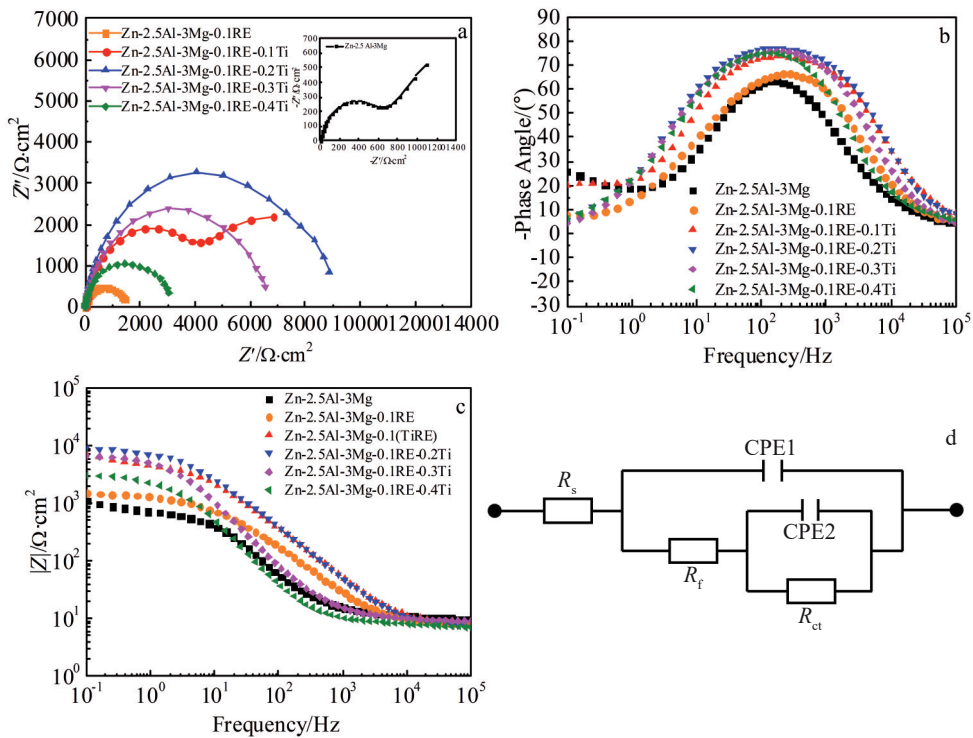


Fig.6 EIS results of Zn-2.5Al-3Mg, Zn-2.5Al-3Mg-0.1RE and Zn-2.5Al-3Mg-0.1RE-xTi alloys in 3.5wt% NaCl solution: (a) Nyquist diagrams, (b) Bode phase angle diagrams, (c) Bode impedance diagrams, and (d) equivalent circuit

Table 3 Equivalent circuit parameters obtained via fitting the EIS data of alloys

Sample	$R_s/\Omega \cdot \text{cm}^2$	$\text{CPE}_1/\Omega^{-1} \cdot \text{s}^{-n_1} \cdot \text{cm}^2$	n_1	$R_f/\Omega \cdot \text{cm}^2$	$\text{CPE}_2/\Omega^{-1} \cdot \text{s}^{-n_2} \cdot \text{cm}^2$	n_2	$R_{ct}/\Omega \cdot \text{cm}^2$	$\lambda^2/\times 10^{-4}$
Z (Zn-2.5Al-3Mg)	9.69	4.4654×10^{-5}	0.809 92	766.1	1.6374×10^{-3}	1	774	15.55
Z-0.1RE	8.354	2.1794×10^{-5}	0.855 76	591.6	2.463×10^{-4}	0.374 9	113 2	5.223
Z-0.1RE-0.1Ti	8.153	8.6346×10^{-6}	0.887 15	315 1	9.6009×10^{-5}	0.568 35	354 8	3.227
Z-0.1RE-0.2Ti	7.575	8.014×10^{-6}	0.896 81	342 8	4.2349×10^{-5}	0.302 18	687 5	2.993
Z-0.1RE-0.3Ti	9.011	9.8087×10^{-6}	0.898 96	325 5	4.5899×10^{-5}	0.601 05	356 4	1.406
Z-0.1RE-0.4Ti	7.509	2.0649×10^{-5}	0.900 38	116 3	2.7638×10^{-4}	0.699 23	213 0	24.97

lower than that of Zn-2.5Al-3Mg alloy. It suggests that the addition of RE and Ti elements can significantly improve the corrosion resistance of Zn-2.5Al-3Mg alloy. However, it is worth noting that the Zn-2.5Al-3Mg-0.1RE-0.2Ti alloy has

the largest corrosion potential and the smallest corrosion current density among these alloys. This may be due to the more precipitated MgZn_2 phase and the more uniform grain distribution.

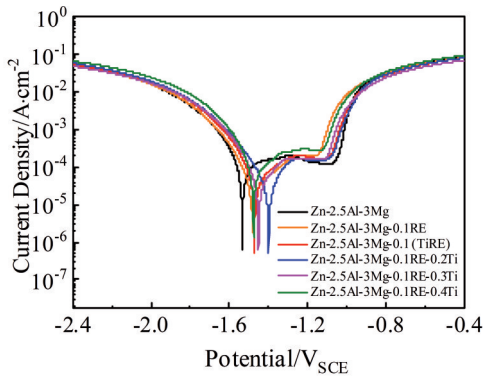


Fig.7 Potentiodynamic polarization curves of Zn-2.5Al-3Mg, Zn-2.5Al-3Mg-0.1RE and Zn-2.5Al-3Mg-0.1RE-xTi alloys in 3.5wt% NaCl solution

Table 4 Electrochemical parameters calculated from potentiodynamic polarization test

Sample	E_{corr}/V	$I_{\text{corr}}/\times 10^{-5} \text{ A}\cdot\text{cm}^{-2}$
Z (Zn-2.5Al-3Mg)	-1.534	12.942
Z-0.1RE	-1.482	3.2589
Z-0.1RE-0.1Ti	-1.471	5.1511
Z-0.1RE-0.2Ti	-1.399	3.1376
Z-0.1RE-0.3Ti	-1.450	4.7686
Z-0.1RE-0.4Ti	-1.477	8.8418

2.4 Characterization of corrosion products

The corrosion products of Zn-2.5Al-3Mg, Zn-2.5Al-3Mg-0.1RE and Zn-2.5Al-3Mg-0.1RE-0.2Ti alloys immersed in 3.5wt% NaCl solution were analyzed by XPS. The results are displayed in Fig. 8. It can be seen that C, O, Zn, Al, Mg elements are present in all three alloys, while the added RE and Ti elements are not detected, probably because the added amount is too small or cross-section is small. The narrow spectra of C, O, Zn, Al, Mg elements are fitted by Avantage software. In addition, at a binding energy of 284.8 eV, the charge shift in the measured XPS spectra is corrected for the C 1s peak of the adventitious carbon. In Fig. 8a, carbon exists in two forms in the Zn-2.5Al-3Mg alloy: (1) C-C bond with binding energy of 284.82 eV, which is from adventitious carbon contaminants, and (2) O-C=O bond with binding energy of 289.22 eV. However, carbon exists in four ways: C-C, C-O-C, O-C=O and carbonates in the Zn-2.5Al-3Mg-0.1RE and Zn-2.5Al-3Mg-0.1RE-0.2Ti alloys (Fig. 8b and 8c) [29-30]. Fig. 8d-8f present the O 1s spectra of Zn-2.5Al-3Mg, Zn-2.5Al-3Mg-0.1RE and Zn-2.5Al-3Mg-0.1RE-0.2Ti alloys, respectively. In the Zn-2.5Al-3Mg alloy, the O 1s spectra benefit from two contributions: hydroxides and metal oxides. In Fig. 8e and 8f, the O 1s spectrum contains three peaks, at the binding energy of 532.07, 531.33 and 530.16 eV (approximately), corresponding to hydroxides, carbonates and metal oxides, respectively [6].

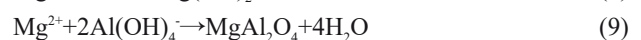
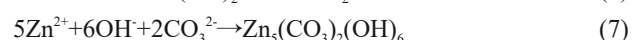
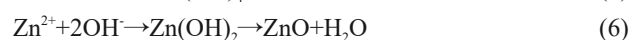
Analysis of the Zn $2p_{3/2}$ spectrum (Fig. 8g) indicates the presence of Zn(OH)₂ and ZnO in the Zn-2.5Al-3Mg alloy.

Nevertheless, Zn mainly exists in the form of hydrozincite Zn₅(CO₃)₂(OH)₆ in Zn-2.5Al-3Mg-0.1RE alloy (Fig. 8h). As shown in Fig. 8i, Zn is found in two chemical states for Zn-2.5Al-3Mg-0.1RE-0.2Ti alloy, which are hydrozincite Zn₅(CO₃)₂(OH)₆ and spinel oxides ZnAl₂O₄ [31-32]. Fig. 8j-8l exhibit the XPS spectra of the Al 2p of the three alloys. Two different peaks are found (Fig. 8j), i.e. aluminum metal (Al⁰) and oxidized aluminum (Al³⁺). For Zn-2.5Al-3Mg-0.1RE and Zn-2.5Al-3Mg-0.1RE-0.2Ti alloys, the Al 2p spectra all have one peak, at the binding energy of 74.05 and 74.03 eV respectively, which indicates the presence of Al₂O₃ [32-33]. As for the spectrum of Mg 1s in Fig. 8m, it reveals the presence of one component, mostly Mg(OH)₂ at around 1302.89 eV. The Mg 1s peak is centered at 1304 eV, a binding energy value close to MgAl₂O₄, for both Zn-2.5Al-3Mg-0.1RE and Zn-2.5Al-3Mg-0.1RE-0.2Ti alloys in Fig. 8n-8o.

In summary, the corrosion products of the investigated Zn-2.5Al-3Mg alloy are composed of Zn(OH)₂/ZnO, Al₂O₃, Al metal and Mg(OH)₂. The corrosion products of Zn-2.5Al-3Mg-0.1RE alloy mainly consist of hydrozincite Zn₅(CO₃)₂(OH)₆, Al₂O₃ and MgAl₂O₄. The corrosion products are composed of hydrozincite Zn₅(CO₃)₂(OH)₆, ZnAl₂O₄, Al₂O₃ and MgAl₂O₄ in the Zn-2.5Al-3Mg-0.1RE-0.2Ti alloy. It can be observed that the corrosion products change greatly after the addition of RE element. Compared with Zn-2.5Al-3Mg-0.1RE alloy, the corrosion products of the alloy added with Ti element change slightly. In the initial stage of corrosion, the open circuit potential of MgZn₂ is low, and it acts as the anode to release Zn²⁺ and Mg²⁺. Oxygen is reduced in the cathode region to generate hydroxide ions. In addition, carbon dioxide in the air enters the solution and reacts to produce carbonate ions [33].



Zn²⁺ cannot only react with OH⁻ to form Zn(OH)₂, but also react with OH⁻ and CO₃²⁻ simultaneously to form hydrozincite Zn₅(CO₃)₂(OH)₆. Zn(OH)₂ can be further decomposed into ZnO with loose pores and low adhesion. However, Mg²⁺ will also react with OH⁻ to form Mg(OH)₂. Subsequently, with the increase in OH⁻, the pH value increases. The electrode potential of Al is lower than that of Zn in the alkaline solution. Al acts as the anode to react with OH⁻ to form Al(OH)₄⁻, while the Zn is protected as the cathode [34]. Finally, Zn²⁺ and Mg²⁺ react with Al(OH)₄⁻ to form ZnAl₂O₄ and MgAl₂O₄ with spinel structure, respectively.



Zn₅(CO₃)₂(OH)₆ has a compact structure and can adhere to

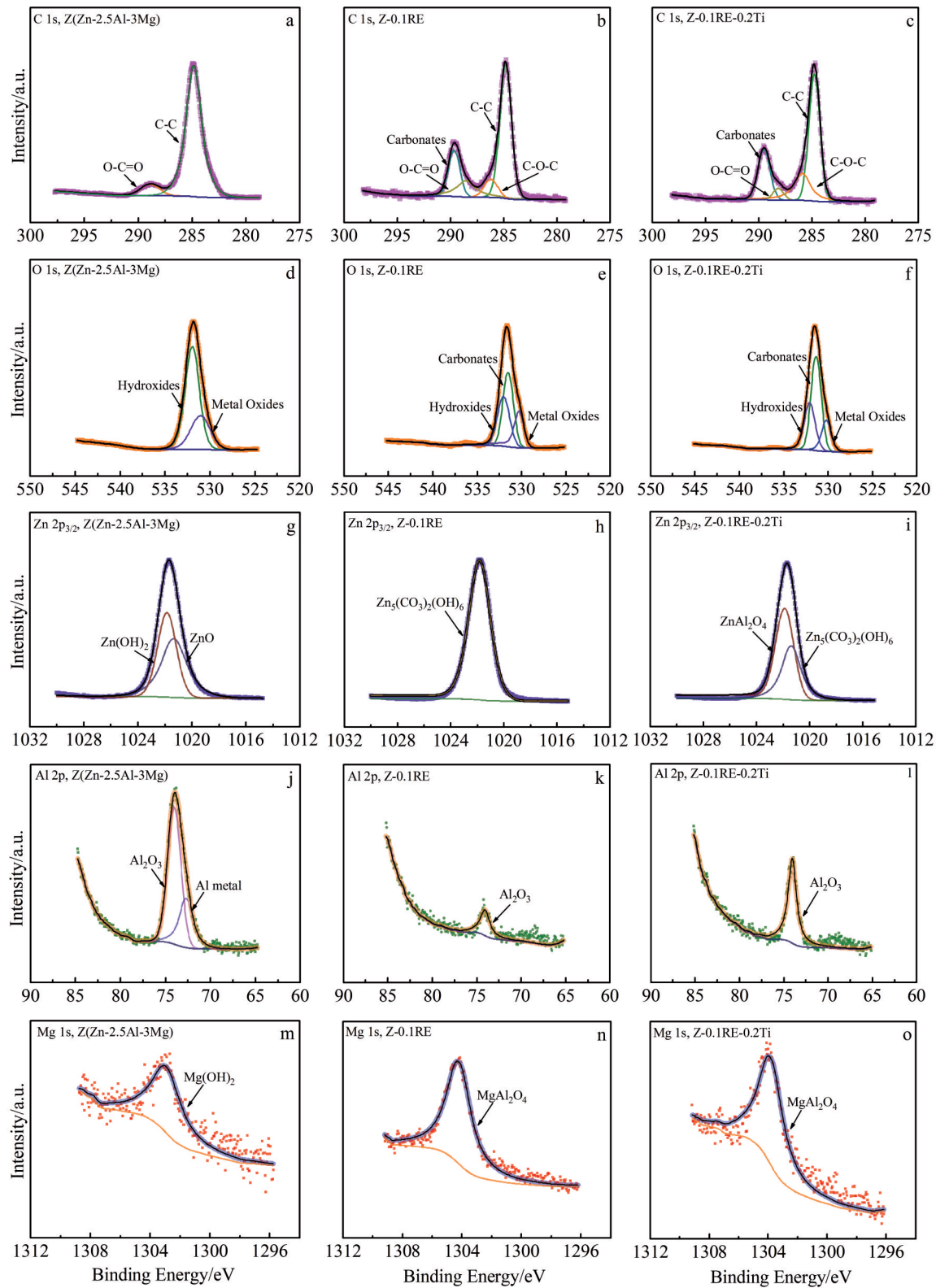


Fig.8 XPS spectra of Zn-2.5Al-3Mg, Zn-2.5Al-3Mg-0.1RE and Zn-2.5Al-3Mg-0.1RE-0.2Ti alloys: (a–c) C 1s, (d–f) O 1s, (g–i) Zn $2p_{3/2}$, (j–l) Al 2p, and (m–o) Mg 1s

the surface of the alloy well, thereby slowing down the corrosion of the alloy^[35]. Related research^[36] reveals that $ZnAl_2O_4$ and $MgAl_2O_4$ with spinel structure in the alloys are useful for improving the corrosion resistance. Noticeably, the addition of RE and Ti elements inhibits the formation of

ZnO and promotes the formation of $Zn_5(CO_3)_2(OH)_6$ and $MgAl_2O_4$. In addition, spinel $ZnAl_2O_4$ is also found in corrosion products of alloys containing Ti element. This indicates that adding RE and Ti at the same time can improve the corrosion resistance of the alloys more significantly than

adding RE element alone. Therefore, the corrosion resistance of Zn-2.5Al-3Mg alloy is greatly improved by adding RE and Ti elements.

3 Conclusions

1) The microstructure of the Zn-2.5Al-3Mg alloy is composed of Zn-rich phase, Zn-MgZn₂/Mg₂Zn₁₁ binary eutectic and Zn/Al/Mg₂Zn₁₁ ternary eutectic. Zn-2.5Al-3Mg-0.1RE alloy consists of Zn-rich phase, (Ce_{1-x}La_x)Zn₁₁ (x=0.41) phase, Zn-MgZn₂/Mg₂Zn₁₁ binary eutectic and Zn/Al/Mg₂Zn₁₁ ternary eutectic. Zn-2.5Al-3Mg-0.1RE-xTi alloy is composed of Zn-rich phase, Al-rich phase, Al₂Ti phase, Zn-MgZn₂/Mg₂Zn₁₁ binary eutectic and Zn/Al/Mg₂Zn₁₁ ternary eutectic.

2) The addition of RE element does not change the size of the binary eutectic. However, the binary eutectic size of alloys containing Ti element is greatly reduced. Among these alloys, when the addition amount is 0.2%, the size is the smallest, the number of MgZn₂ is the largest, and the structure distribution is uniform.

3) Among the six tested alloys, the Zn-2.5Al-3Mg-0.1RE-0.2Ti alloy has the highest surface product resistance R_p and charge transfer resistance R_{ct} values, and its corrosion potential is the most positive and the corrosion current density is the smallest, indicating that the Zn-2.5Al-3Mg-0.1RE-0.2Ti alloy has the best corrosion resistance.

4) The corrosion products of Zn-2.5Al-3Mg alloy include Zn(OH)₂/ZnO, Al₂O₃, Al metal and Mg(OH)₂. The corrosion products are composed of Zn₅(CO₃)₂(OH)₆, Al₂O₃ and MgAl₂O₄ in Zn-2.5Al-3Mg-0.1RE alloy. Compared with the Zn-2.5Al-3Mg-0.1RE alloy, the corrosion products of the alloy containing Ti element have ZnAl₂O₄, Zn₅(CO₃)₂(OH)₆, ZnAl₂O₄ and MgAl₂O₄ can be well attached to the surface of the sample, which provides a certain barrier for the corrosion of the sample, thereby slowing down the corrosion rate of the alloy.

References

- Wang Huaitao, Liu Zili, Xu Wenlong et al. *Corrosion Protection*[J], 2013, 34(2): 133 (in Chinese)
- Liu Anqiang, Xiao Kui, Li Xiaogang et al. *Thermal Spray Technology*[J], 2015, 7(4): 46 (in Chinese)
- Qiao Tengbo. *Study of Process and Corrosion Mechanism of Hot-Dip Galvan Coating*[D]. Tianjin: Hebei University of Technology, 2014 (in Chinese)
- Gao Qiuzhi. *Research on Microstructure and Process of Hot-Dipping Galvan Coating by Sendzimir*[D]. Tianjin: Hebei University of Technology, 2009 (in Chinese)
- Prosek T, Persson D, Stoullil J et al. *Corrosion Science*[J], 2014, 86: 231
- Wang Yanqi, Kong Gang, Che Chunshan. *Corrosion*[J], 2019, 75(2): 203
- Prosek T, Hagström J, Persson D et al. *Corrosion Science*[J], 2016, 110: 71
- Lin Anbang. *Study on the Microstructure and Performance of Hot Dipping Zn-6Al-3Mg Alloy Coating*[D]. Tianjin: Hebei University of Technology, 2014 (in Chinese)
- Sohn I R, Kim T C, Ju G I et al. *Corrosion Science Technology*[J], 2021, 20(1): 7
- Li Shiwei, Gao Bo, Yin Shaohua et al. *Applied Surface Science*[J], 2015, 357: 2004
- Guo Kai, Li Xingeng, Wang Xiaoming et al. *International Journal of Electrochemical Science*[J], 2016, 11: 5063
- Han Yu, Xia Yanqiu, Chen Xin et al. *Anti-corrosion Methods and Materials*[J], 2018, 65(2): 131
- Yang Sui, Su Xuping, Wang Jianhua et al. *Journal of Alloys and Compounds*[J], 2010, 499: 194
- Gui Yan, Xu Qiaoyu. *Electroplating Finishing*[J], 2009, 28(3): 21 (in Chinese)
- Dong Xueqiang, Guo Taixiong, Li Feng et al. *Materials Protection*[J], 2015, 48(8): 63 (in Chinese)
- Cui Jun, Liu Zili, Liu Xiqin et al. *Corrosion Protection*[J], 2018, 39(4): 294 (in Chinese)
- Yao Caizhen, Lv Haibing, Zhu Tianping et al. *Journal of Alloys and Compounds*[J], 2016, 670: 239
- Gogola P, Gabalcová Z, Kusý M et al. *Materials*[J], 2021, 14(18): 5404
- Bruycker E D, Zermout Z, Cooman B C D. *Materials Science Forum*[J], 2007, 58(539-543): 1276
- Li Li, Liu Yongchang, Gao Huixia et al. *Journal of Materials Science-Materials in Electronics*[J], 2013, 24(1): 336
- Veys-Renaux D, Guessoum K, Rocca E et al. *Corrosion Science*[J], 2013, 77: 342
- Li Kailiang, Wu Changjun, Peng Haoping et al. *Chinese Journal of Engineering*[J], 2016, 38(8): 1123 (in Chinese)
- Volovitch P, Allely C, Ogle K. *Corrosion Science*[J], 2009, 51(6): 1251
- Rai P K, Rout D, Kumar D S et al. *Journal of Materials Engineering and Performance*[J], 2021, 30(6): 4138
- Chen Lin, Chen Changguo, Wang Ningning et al. *Rare Metal Materials and Engineering*[J], 2015, 44(2): 333
- Zhou Hanyu, Hou Ruiqing, Yang Junjie et al. *Journal of Alloys and Compounds*[J], 2020, 840: 155 792
- Xu Minyun, Han Dong, Zheng Zhaoyang et al. *Surface and Coatings Technology*[J], 2022, 444: 128 665
- Jia Zheng, Yu Bing, Fu Li. *Rare Metal Materials and Engineering*[J], 2023, 52(2): 568 (in Chinese)
- Schürz S, Luckeneder G H, Fleischanderl M et al. *Corrosion Science*[J], 2010, 52(10): 3271
- Ye Chengtong, Jia Lina, Xu Gaoxiang et al. *Surface and Coatings Technology*[J], 2019, 366: 214
- Duchoslav J, Kehrer M, Truglas T et al. *Applied Surface Science*[J], 2020, 504: 144 457
- Duchoslav J, Steinberger R, Arndt M et al. *Corrosion Science*[J], 2015, 91: 311
- Zhou Shengguo, Yan Qingqing, Tang Chutian et al. *Corrosion*

- Science[J], 2019, 163: 108-254
- 2015, 90: 482
- 34 Hao Yulin, Shen Hai, Zhao Yi. *Paint and Coatings Industry*[J], 2018, 48(12): 7 (in Chinese)
- 36 Zhu Zixin, Chen Dong, Xu Binshi. *International Conference on Mechanical Materials and Manufacturing Engineering*[C]. Switzerland: Trans Tech Publications, 2011: 727
- 35 Azevedo M S, Allely C, Ogle K et al. *Corrosion Science*[J],

添加RE和Ti元素对Zn-2.5Al-3Mg合金微观结构和耐腐蚀性能的影响

陈文萱¹, 周国荣¹, 王学锋¹, 马龙悦¹, 赵德刚¹, 李永生², 王 栋², 秦碧莲³

(1. 济南大学 材料科学与工程学院, 山东 济南 250022)

(2. 山东省建筑工程质量检验检测中心有限公司, 山东 济南 250031)

(3. 山东省环科院环境工程有限公司, 山东 济南 250013)

摘要: 采用XRD、SEM、TEM和XPS等研究了RE和Ti元素对Zn-2.5Al-3Mg合金微观结构和耐蚀性的影响。结果表明, Zn-2.5Al-3Mg合金的微观结构由富Zn相、二元共晶($Zn-MgZn_2/Mg_2Zn_{11}$)和三元共晶($Zn/Al/Mg_2Zn_{11}$)组成, 而含有RE和Ti元素的合金中出现了新相($Ce_{1-x}La_xZn_{11}$ 和 Al_2Ti)。电化学阻抗谱表明, 相对于Zn-2.5Al-3Mg合金, Zn-2.5Al-3Mg-0.1RE-0.2Ti合金的耐蚀性得到了显著提高。XPS分析结果表明, RE元素的添加促进腐蚀产物 $Zn_3(CO_3)_2(OH)_6$ 和 $MgAl_2O_4$ 的形成, 而RE和Ti元素的同时添加促进腐蚀产物 $Zn_3(CO_3)_2(OH)_6$ 、 $ZnAl_2O_4$ 和 $MgAl_2O_4$ 的形成, 且都抑制了疏松多孔ZnO的生成。 $Zn_3(CO_3)_2(OH)_6$ 、 $ZnAl_2O_4$ 和 $MgAl_2O_4$ 能够很好地粘附在试样表面, 提供一层致密的保护层, 从而提高Zn-2.5Al-3Mg合金的耐腐蚀性。

关键词: Zn-Al-Mg合金; 耐腐蚀性; 电化学; XPS

作者简介: 陈文萱, 女, 1999年生, 硕士, 济南大学材料科学与工程学院, 山东 济南 250022, E-mail: 1842284001@qq.com